CALDose_X—a software tool for the assessment of organ and tissue absorbed doses, effective dose and cancer risks in diagnostic radiology

2008 Phys. Med. Biol. 53 6437

(http://iopscience.iop.org/0031-9155/53/22/011)

IOP PUBLISHING PHYSICS IN MEDICINE AND BIOLOGY

Phys. Med. Biol. **53** (2008) 6437–6459 doi:10.1088/0031-9155/53/22/011

CALDose_X—a software tool for the assessment of organ and tissue absorbed doses, effective dose and cancer risks in diagnostic radiology

R Kramer[1], **H J Khoury**[1] **and J W Vieira**[2,3]

[1] Departamento de Energia Nuclear, Universidade Federal de Pernambuco, Av. Prof. Luiz Freire 1000, Cidade Universitária, CEP 50740-540, Recife, PE, Brazil
[2] Centro Federal de Educação Tecnológica de Pernambuco, Recife, PE, Brazil
[3] Escola Politécnica, UPE, Recife, PE, Brazil

E-mail: rkramer@uol.com.br

Received 30 June 2008, in final form 29 September 2008
Published 21 October 2008
Online at stacks.iop.org/PMB/53/6437

Abstract

CALDose_X is a software tool that provides the possibility of calculating incident air kerma (INAK) and entrance surface air kerma (ESAK), two important quantities used in x-ray diagnosis, based on the output of the x-ray equipment. Additionally, the software uses conversion coefficients (CCs) to assess the absorbed dose to organs and tissues of the human body, the effective dose as well as the patient's cancer risk for radiographic examinations. The CCs, ratios between organ or tissue absorbed doses and measurable quantities, have been calculated with the FAX06 and the MAX06 phantoms for 34 projections of 10 commonly performed x-ray examinations, for 40 combinations of tube potential and filtration ranging from 50 to 120 kVcp and from 2.0 to 5.0 mm aluminum, respectively, for various field positions, for 29 selected organs and tissues and simultaneously for the measurable quantities, INAK, ESAK and kerma area product (KAP). Based on the x-ray irradiation parameters defined by the user, CALDose_X shows images of the phantom together with the position of the x-ray beam. By using true to nature voxel phantoms, CALDose_X improves earlier software tools, which were mostly based on mathematical MIRD5-type phantoms, by using a less representative human anatomy.

(Some figures in this article are in colour only in the electronic version)

1. Introduction

It is well known that exposures resulting from radiological procedures contribute the largest part to the population exposure from artificial sources. For this reason, it is necessary to minimize organ and tissue absorbed doses arising from these procedures and to optimize their application. Patient dosimetry in x-ray diagnosis is usually based on the determination of the

entrance surface air kerma (ESAK) in the center of the x-ray beam because of the simplicity of its measurement. In some cases, this information is sufficient for the establishment and use of guidance or reference levels. For comparative risk assessment however, the average dose to organs and tissues at risk should be assessed. Such data cannot be measured directly in patients undergoing x-ray examinations and are difficult and time consuming to obtain by measurements using physical phantoms, but can easily be assessed in virtual human phantoms using Monte Carlo (MC) methods.

Conversion coefficients between absorbed or equivalent dose to organs at risk and measurable quantities commonly used in x-ray diagnosis have been calculated by MC methods for the last 30 years mostly with mathematical MIRD5-type phantoms. Kramer and Drexler (1976) and Rosenstein (1976) published independently organ doses in the MIRD5 phantom (Snyder *et al* 1974) for diagnostic radiology for the first time. Since then, comprehensive compilations of organ absorbed doses for the most important as well as for special examinations have been published for the ADAM and EVA phantoms (Kramer *et al* 1982) and other MIRD5-type phantoms, relating the quantities of interest to measurable quantities, such as exposure in free air, entrance exposure on the surface of the patient or dose-area product (Jones and Wall 1985, Rosenstein 1988, Drexler *et al* 1990, Le Heron 1992, Hart *et al* 1994, Schultz *et al* 1994, 1995, Petoussi-Henss *et al* 1995).

Until the middle of the ninetiess of the last century, the results of these studies were usually published in reports containing extensive tables with CCs for the most frequent x-ray examinations. Later, software tools for absorbed dose calculation in x-ray diagnosis began to appear.

One of the first tools was published by Rannikko *et al* (1997), who developed a computer program, called WinODS (WinODS 2008), for organ absorbed dose calculations with a size- and sex-adjustable phantom. This method uses analytical functions, based on MC-calculated depth-dose distributions for a semi-infinite homogeneous water slab, and applies them to 35 sagittal slices based on a male ALDERSON-RANDO (AR) (Alderson *et al* 1962) phantom containing contours of organ cross sections. Organ absorbed doses are calculated as sum over the absorbed doses to voxels having a size of 1 cm $\times$ 1 cm $\times$ d, where $d = 2.5$ cm is the slice thickness. A female phantom was derived from the male phantom and underweight as well as overweight male and female versions have also been constructed based on statistics from the Finnish clothing industry. WinODS can easily be adapted to a variety of exposure conditions as well as patient anatomies and the results appear almost instantaneously; however, being based on depth–dose distributions for a homogeneous water phantom, many corrections had to be made for WinODS in order to fit these distributions into the shape and the inhomogeneous structure of the AR phantom. Still, correction factors for shielding by bone were applied only to the ovaries and the uterus for posterior—-anterior and lateral projections and the voxel size is quite large to properly represent small organs and tissues. WinODS calculates the effective dose based on ICRP60 (ICRP 1991) and runs only on WINDOWS 98. According to the distributor (Wendin 2008), there are no plans to update WinODS with respect to the operational system and/or the revised concept of effective dose published by the International Commission on Radiological Protection (ICRP) in its new recommendations ICRP103 (ICRP 2007).

Shortly after, Servomaa and Tapiovaara (1998) published the program PCXMC, which is distributed from a website of the Finnish Radiation and Nuclear Safety Authority (PCXMC 2008). PCXMC is a MC computer code using the whole hermaphrodite MIRD5 phantom family (Cristy 1980) and applying scaling factors to modify the size of the phantoms. As opposed to WinODS, PCXMC is not using pre-calculated data but performing a MC calculation for the exposure conditions defined by the user. Therefore, for a given computer,

organ and tissue absorbed doses are emitted by PCXMC perhaps only after some minutes, depending on the level of statistical accuracy required by the user. The latest version 1.5.2 runs on WINDOWS 95/98/NT/2000/XP and calculates the effective dose based on ICRP60. According to one of the authors (Tapiovaara 2008), PCXMC will be updated to calculate the effective dose based on ICRP103 and the radiation risk.

DoseCal is a software tool published by Kyriou *et al* (2000), which uses the CCs determined by Jones and Wall (1985) and by Hart *et al* (1994) for adult and pediatric MIRD5 phantoms, but this program does not scale a given phantom for weight or size. Using pre-calculated CCs, DoseCal outputs results almost instantaneously. DoseCal calculates the effective dose based on ICRP60 and runs only on WINDOWS 98. According to one of the authors (Kyriou 2008), there are no plans to update DoseCal with respect to the operational system and/or the revised concept of effective dose published by ICRP in its new recommendations ICRP103 (ICRP 2007).

The development of tomographic or voxel-based phantoms began in the 80s of the last century (Williams *et al* 1986) in order to overcome the inadequate anatomy of the MIRD5-type phantoms, but relatively few studies with respect to diagnostic radiology have been published with voxel-based phantoms over the last 22 years (Zankl *et al* 2000, Akahane *et al* 2001, Winslow *et al* 2004, Petoussi-Henss *et al* 2005, Bozkurt and Bor 2007) and then they are mainly about special radiographic examinations. None of them presented a comprehensive set of voxel-based CCs for the most important x-ray examinations and no corresponding software tool had been developed so far, i.e. after having been upgraded, PCXMC would then be the only software tool available for x-ray diagnosis but still only based on hermaphroditic MIRD5 phantoms, which are poor representations of human anatomy and do not allow for a sex-specific absorbed dose calculation of the effective dose according to ICRP103.

The purpose of this study is, therefore,

(a) to calculate organ and tissue CCs for the most common examinations in x-ray diagnosis with the recently developed MAX06 and FAX06 voxel phantoms for various projections and different x-ray spectra,
(b) to make these CCs available to the public through a software tool, called CALDose_X (*CAL*culation of *Dose* for *x*-ray diagnosis), to be used in daily routine work by radiological departments of hospitals, health services, regulatory authorities, educational programs, etc, for the assessment of the incident air kerma (INAK), the ESAK and organ and tissue absorbed doses for x-ray examinations and exposure conditions defined by the user, by multiplying the CCs with the value of the corresponding measurable quantity, for determining the effective dose with sex-specific phantoms according to ICRP103 and for estimating the patient's cancer risks.

Earlier publications have reported about the development and the use of the MAX06 and the FAX06 phantoms, the methods of calculation (Kramer *et al* 2003a, 2004a, 2004b, 2005a, 2005b, 2006a, 2006c, 2007) and about comparisons with data from other phantoms, also covering the area of x-ray diagnosis (Kramer *et al* 2003b, Vieira *et al* 2003, Lima *et al* 2003, 2004, Kramer *et al* 2006b). Consequently, this study will refer to the underlying scientific methods only as far as it is necessary for the understanding of the program CALDose_X. For specific issues, the reader is kindly asked to consult the references.

2. Materials and methods

2.1. The MAX06 and the FAX06 phantoms

MAX06 and FAX06 (Kramer *et al* 2006a) are updated versions of the MAX (Kramer *et al* 2003a) and of the FAX phantoms (Kramer *et al* 2004a). The update became necessary

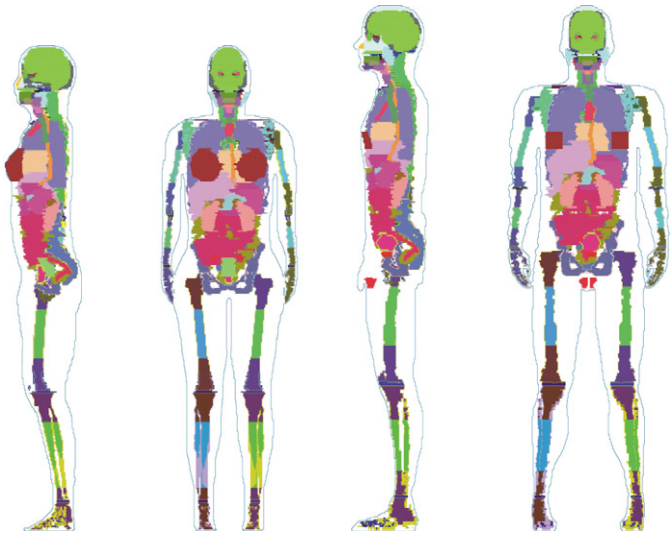

Figure 1. The FAX06 and the MAX06 phantoms (adipose and muscle tissues removed).

because of the inclusion of the extra-thoracic airways, the oral mucosa, the gall bladder, the heart, the lymphatic nodes, the prostate, the salivary glands and male breasts into the concept of effective dose (ICRP 2007). The updated phantoms are made of a 1.2 mm cubic voxel, and the additional segmentation was based on the original CT images from which the MAX/FAX phantoms had been developed, on anatomical textbooks and on skeletal data provided by ICRP70 (ICRP 1995) and ICRP89 (ICRP 2003). Like MAX and FAX, the MAX06 and the FAX06 phantoms have organ and soft tissue masses in accordance with the reference data from ICRP89. Soft, muscle, adipose, skin, lung and cartilage tissue as well as a homogeneous mixture for the skeleton have been used in organs and tissues of the two phantoms. The elemental compositions and densities were taken from or are based on data given in ICRU44 (ICRU 1989), except for the composition of the skeletal mixture which has been taken from the report of Cristy and Eckerman (1987). The most important soft tissue organs and the skeletons of the two phantoms are shown in figure 1.

2.2. The EGSnrc Monte Carlo code

The EGSnrc MC code (Kawrakow 2000), in the form of version V4-r2-2-3 (Kawrakow 2006), was used to calculate organ and tissue absorbed doses in the FAX06 and the MAX06 phantoms. The EGSnrc system, which provides a much improved implementation of the condensed history technique for charged particle transport and uses single scattering simulation in the vicinity of interfaces between different materials, is much better suited for the simulation of particle transport in small regions compared to its predecessor EGS4 (Nelson *et al* 1985). In addition, EGSnrc includes Doppler broadening and binding corrections in the simulation of Compton scattering and simulates the full relaxation cascade of inner shell vacancies, thus, providing more reliable results at low photon energies. EGSnrc simulates coupled electron–photon transport through arbitrary media.

2.3. Absorbed dose and normalization quantities

2.3.1. Organ and tissue absorbed dose. For each MC simulation of a diagnostic x-ray examination, average absorbed doses (kerma) have been calculated in the following 29 organs and tissues of the MAX06 and the FAX06 phantoms: adrenals, bladder wall, brain, oral mucosa, colon wall, breasts, kidneys, liver, lungs, muscle tissue, esophagus, ovaries, testes, pancreas, small intestine wall, skin, spleen, stomach wall, salivary glands, thymus, thyroid, extra-thoracic region, uterus, prostate, heart wall, lymphatic nodes, gall bladder wall, bone surface cells (BSC) and red bone marrow (RBM). Absorbed dose to the mouth cavity was taken as surrogate absorbed dose to the oral mucosa. The 29 organs and tissues are those specified by the ICRP for the calculation of the effective dose (ICRP 2007).

Absorbed dose to skeletal soft tissues. Diagnostic x-ray spectra have normally peak potentials below 150 kV, which translates into secondary electron ranges of less than 0.28 mm in soft tissue, 0.16 mm in cortical bone, 1.1 mm in lung tissue and 0.26 mm in skin tissue, and since the probability of Bremsstrahlung production is very low, it is assumed that the energy of the secondary electron is totally absorbed at the interaction site, i.e. the absorbed dose will be approximated by the kerma. In the energy range below 150 keV, kerma approximation is therefore sufficiently accurate for the average absorbed dose to the skin, the lungs and all soft tissue organs; however, for the absorbed dose to the RBM and to the BSC, those soft tissues which are located in cavities of trabecular bone with diameters in the range between 50 and 2000 μm, secondary electrons, especially those released in trabecular bone, cannot be neglected.

Calculations of RBM and BSC absorbed dose for external exposure to photons based on secondary electron transport in μCT images of trabecular bone have been presented earlier (Kramer *et al* 2006c, 2007). Nevertheless, for the time being, the present study continues to use the older 3 correction factor (3CF) method, which is based on the energy deposited in a homogeneous mixture of marrow and bone in all parts of the skeleton, to which then three correction factors are applied to get an estimate for the RBM absorbed dose. The average absorbed dose to the skeleton is taken as an estimate for the absorbed dose to the BSC. It has been shown that skeletal dosimetry with the 3CF method represents a conservative assessment, i.e. for external exposure to photons below 150 keV, the 3CF RBM and the 3CF BSC absorbed doses are usually greater than the corresponding data determined with μCT images (Kramer *et al* 2006c). The μCT image-based method is still an ongoing project. Therefore, it will be added to the x-ray diagnostic MC code once some remaining open questions have been answered. In the meantime, with the 3CF method, RBM and BSC absorbed doses are on the safe side.

Average absorbed dose. Diagnostic x-ray examinations represent quite inhomogeneous exposures to the human body. Depending on its location with respect to the boundaries of the irradiated body volume, a specific organ or tissue can be exposed by primary radiation completely, partly or not at all. From the assumption of a linear, non-threshold, dose–response relationship (ICRP 2007) follows the concept of average absorbed dose and this study applies this concept to all of the above-mentioned organs and tissues independent from their location with respect to the beam boundaries, except for the RBM, the BSC and the skin. Among the tissues which are distributed over the whole body, the RBM, the BSC and the skin have the greatest risk factors. For example, they are listed in the main group of tissues which are to be taken into account for the determination of the effective dose (ICRP 2007), the RBM being among those tissues with the greatest tissue weighting factor.

Bones, and with them the RBM and the BSC, are distributed very heterogeneously throughout the human body. For diagnostic x-ray examinations, the average whole body RBM or BSC absorbed doses are usually much smaller than the absorbed doses to those parts of these skeletal tissues which are located inside the irradiated volume of the body. Consequently, in this study the absorbed doses to the RBM and the BSC are determined as maximum average absorbed doses selected from the RBM and BSC absorbed doses to the skull, the mandible, the ribcage (ribs, sternum, clavicles and scapulae), the spine, the pelvis, upper arm bones and upper leg bones. Depending on the x-ray projection, it can still happen that some of these bones or bone groups are located partly inside or outside the beam. Therefore, CALDose_X outputs these RBM and BSC absorbed doses as 'mainly in beam volume', which makes them more suitable for risk estimates than the RBM and BSC absorbed doses averaged over the whole body.

Similar considerations apply to the skin. For extreme partial body exposures, like in interventional radiology, even tissue damage may occur, while at the same time, the average whole body skin absorbed dose is still relatively small. In this study, a maximum skin entrance absorbed dose is determined, which is the average absorbed dose to a 7.2 cm × 7.2 cm square of skin tissue centered around the central axis of the beam where it enters the phantom. This quantity is considered to be more appropriate for risk estimates than the skin absorbed dose averaged over the whole body surface.

2.3.2. Normalization quantities. In order to be helpful for diagnostic radiology, organ and tissue absorbed doses determined for human phantoms have to be normalized to measurable quantities. Over the years, many normalization quantities have been used, such as exposure at skin entrance, entrance surface dose or kerma and others, sometimes free-in air or sometimes including backscattered radiation. Clarification and guidance for this issue can be found in report ICRU74 (ICRU 2005) which deals with patient dosimetry in x-ray diagnosis. According to the concepts outlined in that report, CALDose_X presents organ and tissue absorbed doses normalized to the following measurable quantities:

(a) *Incident air kerma.* 'The incident air kerma is the air kerma from the incident beam on the central x-ray beam axis at the focal spot-to-surface distance, i.e. at the skin-entrance plane. Only the primary radiation incident on the patient or phantom and not the backscattered radiation is included'. (ICRU 2005).
(b) *Entrance surface air kerma.* 'The entrance-surface air kerma is the air kerma on the central x-ray beam axis at the point where the x-ray beam enters the patient or phantom. The contribution of backscattered radiation is included.' (ICRU 2005).
(c) *Air kerma-area product (KAP).* 'The air kerma-area product is the integral of the air kerma free-in-air over the area of the x-ray beam in a plane perpendicular to the beam axis.' (ICRU 2005).

Figure 2 represents the exposure condition of a chest x-ray, one of the most frequently performed radiographic examinations nowadays. Besides some organs of interest, the figure indicates the locations to which the measurable quantities INAK, ESAK and KAP refer.

The normalization quantities INAK, ESAK and KAP are determined during the MC run which calculates the absorbed doses to organs and tissues. Based on the spectral photon fluence, INAK and KAP are calculated using the energy dependent fluence-to-air kerma conversion factor given in ICRP74 (ICRP 1996), while the ESAK is derived from the above-mentioned skin absorbed dose to a 7.2 cm × 7.2 cm square of skin tissue centered on the central x-ray beam axis, by transforming it into air kerma using the ratio between the mass energy-absorption coefficients of air and skin.

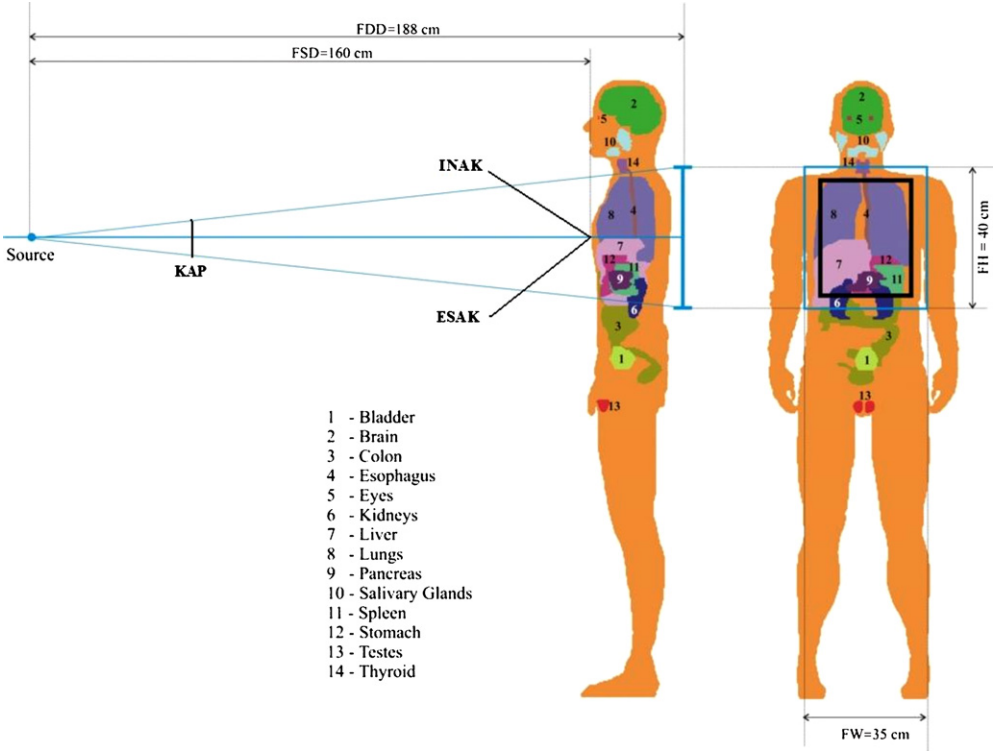

Figure 2. Radiographic exposure of the chest of the MAX06 phantom showing some organs of interest and the locations to which the normalization quantities INAK, ESAK and KAP refer. The larger square represents the field size at the detector plane, the smaller square represents the field size at the entrance surface.

2.4. Diagnostic x-ray examinations

Calculations have been made for 34 projections of the diagnostic x-ray examinations, together with focus-to-surface distances (FSDs) and field sizes in the plane of the image receptor shown in table 1. Typical FSDs and field sizes have been determined from data given in the reports of Rosenstein (1988), Drexler *et al* (1990) and Hart *et al* (1994), comprehensive studies which cover exposure conditions frequently found in the USA, the EC and the UK, respectively. Additional 5 cm were included in the focus-to-detector distance at the exit side of the x-ray beam in order to provide for the space usually occupied by the patient's support table, antiscatter grid and film cassette holder.

The 40 x-ray spectra used were generated from the *Catalogue of Diagnostic x-Ray Spectra and Other Data* IPEM/SR78 by Cranley *et al* (1997) for constant potential generators, x-ray tubes with 17° target angles, peak potentials between 50 and 120 kV and total beam filtrations of 2.0–5.0 mm Al.

The MC calculations have been done with 5 million source photons per examination. Thereby, most organ and tissue absorbed doses in the x-ray beam had a statistical error of 1% or less. CALDose_X runs on WINDOWS 2000/NT/XP/VISTA. Typical runtime was 15 min per examination on a PC with an Intel Pentium 4.2 GHz processor. The database of

Table 1. Diagnostic x-ray examinations.

Examination	Projection	FSD cm	Field size cm × cm
Head	AP, PA	80	24 × 30
Head	RLAT, LLAT	85	30 × 24
Cervical spine	AP	80	18 × 24
Cervical spine	RLAT, LLAT	80	18 × 24
Throat	RLAT, LLAT	75	18 × 24
Thoracic spine	AP	80	20 × 40
Thoracic spine	RLAT, LLAT	70	20 × 40
Chest	AP, PA	160	35 × 40
Chest	RLAT, LLAT	150	25 × 40
Stomach	AP, PA	40	24 × 30
Stomach	RAO, LPO,LAO	40	24 × 30
Lumbar spine	AP	80	20 × 40
Lumbar spine	RLAT, LLAT	70	20 × 40
Lumbar spine	LPO, RPO	70	24 × 30
Duodenum	AP, PA	45	15 × 15
Duodenum	RAO, LPO	45	20 × 20
Abdomen	AP, PA	80	35 × 40
Pelvis/colon	AP, PA	80	40 × 35

FSD = Focus-to-surface distance, Field size = width × height in detector plane, AP = anterior–posterior projection, PA = posterior–anterior projection, RLAT = right lateral projection, LLAT = left lateral projection, RAO = right anterior oblique, LAO = left anterior oblique, RPO = right posterior oblique, LPO = left posterior oblique.

CALDose_X consists of 32160 tables with CCs normalized to INAK, ESAK and KAP for the two phantoms.

2.5. Sources of uncertainty

2.5.1. The phantoms. Compared to the stylized MIRD5 phantoms, FAX06 and MAX06 are true to nature representations of humans, which make their CCs applicable to individual patients, at least to those with similar anatomical properties, if one neglects minor differences that still could exist with regard to organs without fixed positions, such as stomach, colon and small intestine. Among the anatomical properties of adult patients of a given age, the central fat mass (CFM), i.e. the subcutaneous and visceral fat mass of the trunk, can influence organ and tissue absorbed doses significantly, whereas the peripheral fat mass (PFM), i.e. the subcutaneous fat mass of the extremities, has negligible influence at least for the examinations mentioned in table 1. Ketel *et al* (2007) have reported that among the various anthropometric parameters they investigated, the waist circumference showed the best correlation with the CFM, which had been determined before independently by dual-energy x-ray absorptiometry. Body mass index and body weight also showed good correlation, but only with the total (CFM + PFM) fat mass. Measuring the circumference of a patient's waist can easily be done without impeding the patient or the medical procedure. The next version of CALDose_X will be updated with CCs for derived male and female phantoms having different fat distributions. Based on the value for the waist circumference, CALDose_X will then select a patient-specific set of CCs. In the meantime, CALDose_X is using the FAX06 and the MAX06 phantoms for all adult patients.

2.5.2. The statistical error. Increasing the number of photons can reduce the statistical error of the organ and tissue absorbed dose. However, there is a limit to the number of particles that can be calculated, set by the speed of the computer. Here, usually five million photons were used per projection of an x-ray examination, which reduced the statistical error for organs and tissues located inside the beam volume to less than 1% for INAK- and KAP-CCs, and to less than 2% for ESAK-CCs. For organs and tissues located at the boundaries or outside the beam, the statistical error is greater. CALDose_X displays organ and tissue absorbed doses with statistical errors of up to 10%.

2.5.3. Cross-sections and tissue compositions. Uncertainties of cross-sectional data have been reported to be approximately ±2% (Hubbell 1977), which therefore can be ruled out of being a major source of error.

In the FAX06 and the MAX06 phantoms, only one soft tissue composition is used which has been compiled as the average of many organ-specific compositions. It has been shown that differences between soft tissue compositions can cause differences of the effective dose of up to 10% for external exposure to photons for energies below 150 keV (Jones 1995, 1997, Lima *et al* 2004, Kramer *et al* 2004b).

As for the absorbed dose to the RBM and BSC, it has been shown that the data calculated with the homogeneous skeletal mixture are always greater, for energies below 60 keV up to a factor of 2–3, than the data determined with μCT images of trabecular bone. The reason is that in a real skeleton, especially for photon energies below 150 keV, the cortical bone layer and the trabeculae of the spongiosa act as a shield for the soft tissues in the marrow cavities, whereas in the homogeneous skeleton the bone volume contributes also to the absorbed dose (Kramer *et al* 2006c).

2.5.4. Exposure geometry.

Focus-to-surface (FSD) or focus-to-detector (FDD) distance. According to Rosenstein (1988), variation of the FDD by about ±25 cm causes changes of the organ absorbed CCs of less than ±10%. For the FSDs mentioned in table 1, this study found that variation of the FSD by about ±10% causes changes of the CCs of less than ±10% for organs and tissues inside the beam volume. However, organs located on the boundaries of the beam volume, especially small ones, may be found inside or outside the beam after a change of the FSD, which in turn may change the CC by far more than 10%. For the time being, CALDose_X works with one FSD per projection, but the user can apply the inverse square law to the INAK and as a first approximation also to the ESAK to correct for differences of FSDs.

Field size. Many field sizes shown in table 1 represent commercial x-ray film formats. It is assumed that beam collimation is made properly to comply with these formats, i.e., variations of the field size have not been considered here.

Field position. For a given type of examination, projection, x-ray spectrum, FSD and field size, the position of the field on the body is the quantity which has the strongest effect on the absorbed dose of an organ or tissue. Changing the field position only a few centimeters up or down, to the right or to the left can decide if an organ lies inside, outside or on the boundaries of the beam volume. For small organs, such as the testes, a variation of the field position by only 4 cm in an abdominal examination can cause differences for the absorbed dose by up to a factor of four (Jones and Wall 1985). The standard field positions for this study were

chosen based on the location of the organ(s) to be examined and on anatomical landmarks to be visible in the image according to good practice. But one has to be aware about the 'inevitable variations that occur in practice from hospital to hospital and patient to patient' (Jones and Wall 1985). In addition, here the problem is not to calculate CCs for different field positions, but to know in a real situation with a patient if, for example, the testes or the thyroid were inside the beam or not. Therefore, CALDose_X outputs the results for an x-ray examination for the standard field position and also for field positions with a 4 cm shift of the field center in each direction. Thereby, the user gets an idea how organ and tissue absorbed doses would change as a function of the variation of the field center position by 4 cm up or down, to the right or to the left and backward or toward the front.

2.5.5. X-ray spectra. Factors affecting the spectrum shape are

(1) tube peak potential,
(2) tube potential variation during exposure (ripple),
(3) x-ray emission angle,
(4) filtration,
(5) extra focal radiation,
(6) target roughness.

CALDose_X CCs cover the range of 50–120 kVpc for the tube peak potential and of 2.0–5.0 mm Al for the total filtration. A constant potential generator (no ripple) and an x-ray emission angle of 17° have been chosen for the spectra because they represent the most frequent type of generator and target angle found presently in x-ray units.

The effect of extra focal radiation on the spectral shape is insignificant (Birch and Marshall 1979). Target roughness leads to hardening of the x-ray beam and is significant only for aging x-ray tubes. These two factors have not been considered here.

2.5.6. Measurement of the normalization quantities. In order to get an organ absorbed dose estimate, one has to multiply the appropriate CC given by CALDose_X with the value of the INAK, the ESAK or the KAP. Petoussi-Henss *et al* (1995) report that KAP measurements, 'if properly performed, have a 30% uncertainty'. Measurements of INAK or ESAK with TLD dosimeters, for example, show typically uncertainties of about 10–20%. X-ray output measurements with ionization chambers are usually accurate within 10%.

2.6. Effective dose and cancer risk

2.6.1. Effective dose. The concept of effective dose has been introduced by the ICRP for the purpose of radiological protection of workers and the general public (ICRP 2007). The ICRP considers it useful to apply a single value of effective dose to both sexes and to all age groups. Consequently, the tissue weighting factors to be applied to the calculation of the effective dose have been determined as sex- and age-averaged values and therefore the effective dose 'cannot be used for the assessment of individual risk' (ICRP 2007).

Age and gender distributions of patients undergoing radiological examinations can be quite different from the distributions which were used for the derivation of the ICRP tissue weighting factors, and these distributions may differ from one type of medical procedure to another. Therefore, risk assessment in diagnostic radiology should be better based on appropriate risk coefficients for the individual tissues at risk, taking into account age and gender distributions of the individuals undergoing the medical procedure.

As a consequence, the International Commission on Radiation Units and Measurements (ICRU) rejects the use of the effective dose for medical imaging (ICRU 2005) completely, while the International Commission on Radiological Protection (ICRP) considers at least a restricted use of this quantity for diagnostic radiology to be possible:

'Effective dose can be of value for comparing the relative doses from different diagnostic procedures and for comparing the use of similar technologies and procedures in different hospitals and countries as well as the use of different technologies for the same medical examination, provided the reference patient or patient populations are similar with regard to age and sex' (ICRP 2007).

For those who want to determine the effective dose for x-ray examinations, CALDose_X is providing separately calculated weighted MAX06 and FAX06 whole-body absorbed doses, which represent the sex-specific contributions to the effective dose. According to equation 4.5 in ICRP103 (ICRP 2007), the effective dose is then just the arithmetic mean of the two sex-specific weighted absorbed doses.

2.6.2. Cancer risk. If one is interested in quantifying the cancer risk for an individual patient to be submitted to a radiological procedure, one should find the latest age-, sex- and organ- or tissue-specific risk coefficients for cancer incidence and cancer mortality and multiply these coefficients with the average organ or tissue equivalent doses. Following a proposal made by D Brenner (Brenner and Huda 2008), the sum over risk-weighted organs and tissues equivalent doses can be considered as 'whole-body effective risk', given by the equation

$$R = \sum_T r_T H_T,$$

where H_T are the average organ and tissue equivalent doses in tissues T and r_T are the lifetime attributable tissue-specific cancer risks per unit organ equivalent dose.

Tables 2 and 3 show adult risk coefficients for cancer incidence and cancer mortality, respectively, as a function of sex, age and organ taken from the BEIR VII Report (National Research Council 2005). Females have a significantly higher whole-body effective cancer risk than males mainly because of greater risk coefficients not only for the sex-specific organs: breast, uterus and ovaries, but also for the lungs. With aging, risk coefficients decrease for both sexes.

CALDose_X applies the risk coefficients of tables 2 and 3 to calculate sex- and age-specific whole-body risks for cancer incidence and cancer mortality using the equation given above. The organs and tissues considered are those specified in table 3 of ICRP103 (ICRP 2007) for the calculation of the effective dose, which have also been mentioned above in section 2.3.1. The risk coefficient for 'Other' was equally distributed among organs and tissues, which are not mentioned in tables 2 and 3.

The risk coefficients apply to male and female adults between 20 and 80 years of age, whereas the adult anatomical reference values of ICRP89 (ICRP 2003), used for the development of the MAX06 and the FAX06 phantoms, correspond to adult persons of 35 years. Although not being the main focus of the data presented in ICRP89, some information about anatomical changes during adulthood can still be found in the report. With respect to organ mass, no significant changes with increasing adult age have been found for the stomach, the adrenals, the brain and the lungs, while decreases between 15 and 35% have been observed for the spleen, the thymus, the thyroid, the liver, the pancreas and the kidneys for adults between 30 and 80 years of age for both sexes. Partly, the data are based on Asian populations. Loss of trabecular bone mass can amount to 25–45% of the peak trabecular bone mass, while body fat increases by about 12% during the adult life span between 35 and 70 years for both sexes.

Table 2. Lifetime attributable risk of cancer incidence given as number of cases per 100 000 persons exposed to a single dose of 0.1 Gy (National Research Council 2005).

	Age (y)						
Cancer site	20	30	40	50	60	70	80
Males							
Stomach	40	28	27	25	20	14	7
Colon	173	125	122	113	94	65	30
Liver	30	22	21	19	14	8	3
Lungs	149	105	104	101	89	65	34
Prostate	48	35	35	33	26	14	5
Bladder	108	79	79	76	66	47	23
Thyroid	21	9	3	1	0.3	0.1	0
Leukemia	96	84	84	84	82	73	48
Other	312	198	172	140	98	57	23
All cancers	977	686	648	591	489	343	174
Females							
Stomach	52	36	35	32	27	19	11
Colon	114	82	79	73	62	45	23
Liver	14	10	10	9	7	5	2
Lungs	346	242	240	230	201	147	77
Breast	429	253	141	70	31	12	4
Bladder	109	79	78	74	64	47	24
Uterus	26	18	16	13	9	5	2
Ovary	50	34	31	25	18	11	5
Thyroid	113	41	14	4	1	0.3	0
Leukemia	71	63	62	62	57	51	37
Other	323	207	181	148	109	68	30
All cancers	1646	1065	886	740	586	409	214

While body height decreases by about 2% for both sexes, corresponding data for the total body mass are not clear. ICRP89 does not recommend reference values for different adult age groups and the above-mentioned data are mostly presented in figures, which make it difficult to use them as information for changes to be made to organ masses. After all, significant changes of organ mass are more critical for internal dosimetry and less important for external exposures, such as x-ray radiographs. Changes of the bone mass and the trabecular bone structure are important for the absorbed dose to the RBM and the BSC for any type of exposure; however, these can be taken properly into account only after the implementation of a skeletal dosimetry model based on μCT images of spongiosa. Evaluating age-related changes of anatomical parameters during adulthood would be an interesting project for the future. In the meantime, CALDose_X is using the bodies of the '35-year old' MAX06 and FAX06 phantoms for risk estimates for all age groups.

3. Results

3.1. Comparison with other data

3.1.1. MIRD5 phantom. Organ and tissue absorbed doses, shown in table 4, for a lumbar spine radiograph, AP, with 81 kV, 20 mAs, 2.5 mm Al filtration, FSD = 80 cm and a field size in the detector plane of 20 cm × 40 cm, have been calculated with CALDose_X for the MAX06

Table 3. Lifetime attributable risk of cancer mortality given as number of cases per 100 000 persons exposed to a single dose of 0.1 Gy (National Research Council 2005).

	Age (y)						
Cancer site	20	30	40	50	60	70	80
Males							
Stomach	21	16	15	13	11	8	4
Colon	84	61	60	57	49	36	21
Liver	23	16	16	14	12	8	4
Lungs	151	107	107	104	93	71	42
Prostate	9	7	6	7	7	7	5
Bladder	23	17	17	17	17	15	10
Leukemia	67	64	67	71	73	69	51
Other	134	94	88	77	58	36	17
All cancers	511	381	377	360	319	250	153
Females							
Stomach	29	21	20	19	16	13	8
Colon	53	38	37	35	31	25	15
Liver	12	9	8	8	7	5	3
Lungs	305	213	212	204	183	140	81
Breast	101	61	35	19	9	5	2
Bladder	31	23	23	22	22	19	13
Uterus	6	4	4	3	3	2	1
Ovary	28	20	20	18	15	10	5
Leukemia	51	51	52	54	55	52	38
Other	147	103	97	86	69	47	24
All cancers	762	542	507	469	409	317	190

Table 4. Absorbed dose to organs in the MAX06 (CALDose_X) and the MIRD5 (DoseCal) phantoms for a lumbar spine radiograph, AP, with 81 kV, 20 mAs, 2.5 mm Al filtration, FSD = 80 cm and a field size of 20 cm × 40 cm in the detector plane. Mean spectral energy = 42.9 keV. Statistical errors are given in percent in brackets.

Organ	CALDose_X mGy	DoseCal mGy
Adrenals	0.31 (2.1)	0.15 (3.9)
Stomach	1.25 (0.3)	1.04 (1.3)
SMI	1.01 (0.2)	0.70 (1.2)
Colon	0.85 (0.2)	0.61 (1.5)
Kidneys	0.35 (0.4)	0.16 (1.7)
Liver	0.72 (0.1)	0.60 (1.2)
Lungs	0.09 (0.4)	0.05 (1.7)
Pancreas	0.87 (0.4)	0.46 (1.9)
Spleen	0.23 (0.5)	0.22 (2.5)
Bladder	0.34 (1.0)	0.45 (3.2)
RBM	0.06 (0.3)	0.08 (1.1)

SMI = Small intestine, RBM = Red bone marrow.

phantom and with DoseCal, a software based on the hermaphrodite MIRD5 phantom (Kyriou *et al* 2000). Studies on organ and tissue equivalent dose differences between voxel-based and MIRD5-type phantoms for external whole-body exposures to photons have shown that some

Table 5. MAX06 and GOLEM organ and tissue absorbed doses per ESAK and ESD for a pelvic radiograph AP, tube potential = 80 kV, total filtration = 2.5 mm Al, FDD = 115 cm, field size = 38 cm × 35 cm in detector plane, statistical error in percent in brackets.

Organ/tissue	MAX06 AD/ESAK Gy/Gy	GOLEM[a] AD/ESD Gy/Gy
Testes	0.08 (2.0)	0.06
RBM	0.03 (0.2)	0.07
Skeleton	0.13 (0.1)	0.14
Stomach	0.01 (3.0)	0.01
Pancreas	0.01 (2.9)	0.02
SMI	0.29 (1.1)	0.30
Colon	0.18 (1.1)	0.21[b]
ESD	1.52 (1.0)	1.26

AD: Absorbed dose, ESAK: Entrance surface air kerma, SMI: Small intestine, ESD: Entrance surface skin absorbed dose.
[a] Data from Petoussi-Henss *et al* (2005).
[b] Average of upper and lower large intestine.

internal organs have different depths in the two types of phantoms, which causes significant differences of equivalent doses for them (Kramer *et al* 2004b). Medical radiographic exposures are partial-body irradiations, which even increase these differences because now organs can additionally be located inside or outside the beam volume. Comparing the organ absorbed doses for the two phantoms shown in table 4, one has to keep the anatomical differences between them in mind.

For example, the colon of the MIRD5 phantom is a parallelepiped located at the center of the trunk, whereas in the MAX06 phantom the colon spreads out into the frontal part of the abdomen. Consequently, for a spectrum with a mean energy of 42.9 keV, the MAX06 colon receives a higher absorbed dose for AP incidence than the MIRD5 colon. Similar considerations apply to the small intestine. While the MIRD5 bladder begins at a depth of 1 cm below the surface of the body, the same happens for the MAX06 bladder only at a depth of 5 cm. Consequently for AP incidence, the MAX06 bladder absorbed dose is smaller than the MIRD5 bladder absorbed dose. Analysis of the locations of other organs in the two phantoms would correspondingly explain the differences or agreements between the absorbed doses to be observed in table 4.

3.1.2. Voxel-based phantom. From the voxel-based studies mentioned above, only the paper from Petoussi-Henss *et al* (2005) contains tabulated data for the voxel-based phantom GOLEM (Zankl and Wittmann 2001) which can be compared with CCs calculated in this investigation.

Table 5 shows conversion coefficients between organ and tissue absorbed doses and 'entrance dose' for the MAX06 and the GOLEM phantom for a pelvic examination AP, made with 80 kV tube potential, 2.5 mm Al total filtration, FDD = 115 cm and a field size of 38 cm × 35 cm in the plane of the detector.

The small value of the testes CC for the GOLEM phantom indicates that this organ was located outside the beam volume. Therefore, the field position for the MAX06 calculation was adjusted accordingly. From the paper by Petoussi-Henss *et al* (2005), it did not become clear if 'entrance dose' means ESAK or absorbed dose to the skin. The MAX06 absorbed doses are normalized to ESAK. If the GOLEM CCs are normalized to entrance absorbed dose to the skin, then this would introduce additionally a difference of 1.7% between the MAX06 and the GOLEM CCs.

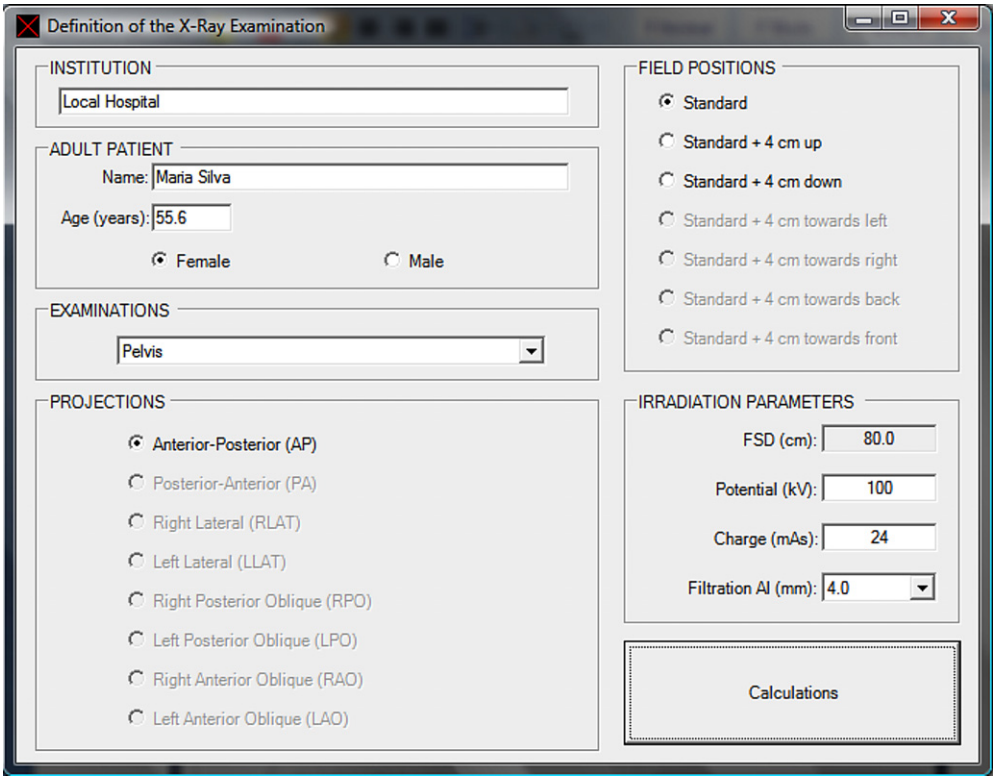

Figure 3. First CALDose_X form: Definition of the x-ray examination.

The numbers in brackets represent the statistical error associated with the MAX06 CCs. For the GOLEM phantom's CCs, no error margins were given. Good agreement can be seen for the testes, the skeleton, the stomach, the small intestine and the colon. RBM absorbed doses differ significantly because both studies use quite different methods for skeletal dosimetry, which has already been discussed by Kramer *et al* (2006c). The skin absorbed dose is calculated as an average absorbed dose in the first voxel layer on the phantom's surface. The size of the MAX06 voxels is 1.2 mm $\times$1.2 mm $\times$1.2 mm, whereas GOLEM's voxels are 2.08 mm $\times$ 2.08 mm $\times$ 8 mm. Consequently, MAX06's skin absorbed dose (ESD) is greater for this range of energies. The two pancreas absorbed doses differ by a factor of two. However, the values are quite small. Rounding errors and/or different organ location can be the cause for this difference. Agreement between MAX06 and GOLEM results is more frequent than between MAX06 and MIRD5 data because the two voxel-based phantoms have similar natural organ and tissue structures compared to the simple geometrical bodies of the MIRD5 phantom.

3.2. The CALDose_X software

This section represents a summary of the user guide, which comes with the download of CALDose_X. Figure 3 shows the first CALDose_X form, where the user can fill in the names of the institution and of the patient. The adult age has to be defined by a number between 20 and 80 and the patient's sex has to be selected. From a drop down window, the user then selects one of the 10 examinations mentioned in table 1. In figure 3, a pelvic radiograph for

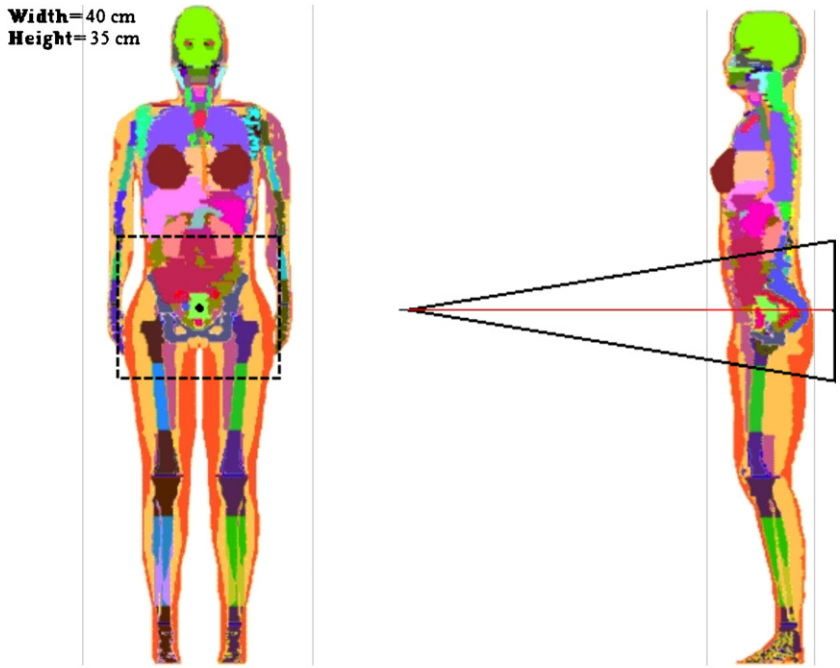

Figure 4. (a) Frontal view of FAX06 phantom with the location and the size of the x-ray field for a pelvic radiograph (b) Lateral view of the FAX06 phantom with the position of the x-ray beam for a pelvic radiograph.

a female patient has been chosen as an example. Next follows the selection of the projection and the position of the field. 'Standard' represents the field location mostly used for this type of examination according to studies mentioned above and based on textbooks for x-ray practitioners. For some examinations, CALDose_X offers alternatively field locations with a 4 cm shift in a certain direction to demonstrate the effect on organ absorbed doses if the field position is 'off Standard'.

Once the field position has been selected, two images pop up, like the examples shown in figures 4(a) and (b), which show the phantom and the position of the x-ray beam relative to the body. Field height and field width are given in centimeters for the plane of the detector (film). These images can be printed and/or saved. For oblique projections, this feature will be added to a later version of CALDose_X. The focus to skin distance (FSD) for the selected examination appears in the first field in the area called 'irradiation parameters'.

Users who only want to visualize the selected examination could close CALDose_X at this point. However, if calculations of ESAK or organ and tissue absorbed doses are requested, then the user has to fill in the tube potential in kV with a number between 50 and 120 and the charge in mAs. Filters between 2 and 5 mm Al can be selected from the drop down window.

After having clicked on the 'Calculations' button, the form shown in figure 5 appears on the screen. The user has now the following options:

(i) *INAK (output).* Calculation of the INAK and the ESAK based on the output of the user's x-ray unit.

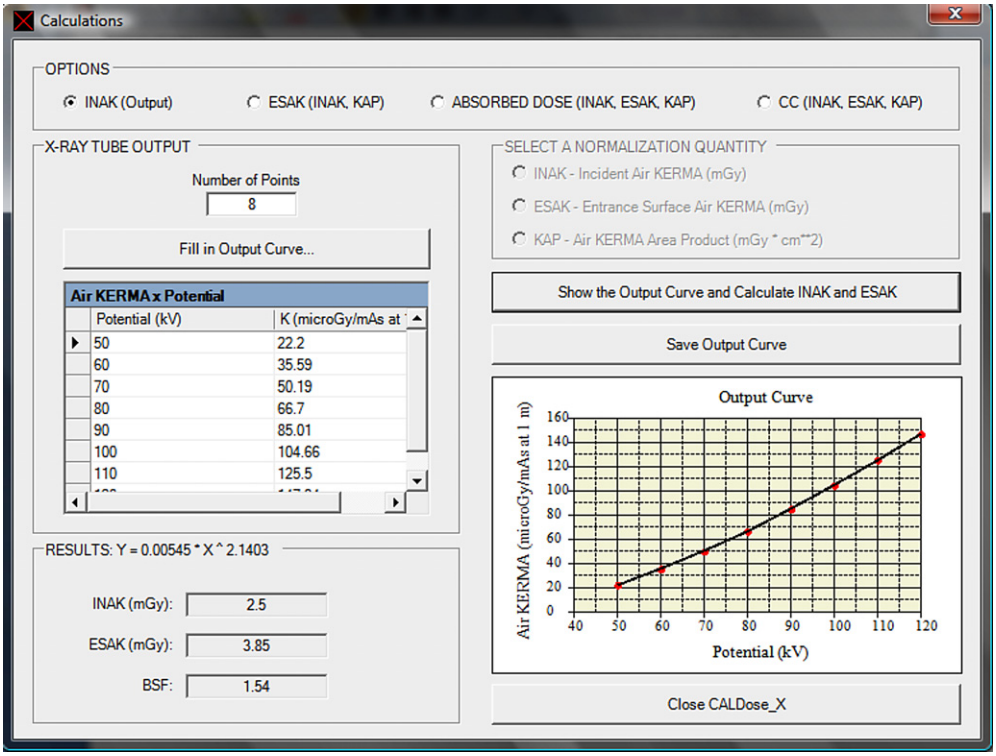

Figure 5. Second CALDose_X form: definition of the type of calculation.

(ii) *ESAK (INAK, KAP).* Calculation of the ESAK based on values for INAK or KAP provided by the user.

(iii) *Absorbed dose (INAK, ESAK, KAP).* Calculation of organ and tissue absorbed doses based on INAK, ESAK or KAP.

(iv) *CC (INAK, ESAK, KAP).* Display of the conversion coefficients.

In the example shown in figure 5, the first option has been chosen, which presumably represents the most frequent case in radiodiagnosis. The user has to inform the values for the tube potential in kV and for the output in μGy/mAs at 1 m distance from the tube. CALDose_X offers the possibility to save the output curve for future calculations. After having clicked on the button 'Show the output curve and calculate INAK and ESAK', CALDose_X shows a graph of the output curve, calculates the INAK and the ESAK for the FSD, potential and charge given by the user and shows the results. The ESAK is the INAK multiplied by the backscatter factor (BSF), which is examination specific and provided by the Monte Carlo calculation.

In a last step, the user should click on the option 'Absorbed Dose (INAK, ESAK, KAP)' and select one of the measurable quantities INAK, ESAK or KAP. The first two are automatically filled in if option (i) or (ii) were selected before. Otherwise, like for the KAP, also for INAK or ESAK, values have to be filled into the corresponding fields seen in figure 6.

A click on 'Calculate Organ and Tissue Absorbed Doses' produces table 6, which shows the name of the institution, the patient's sex, age, name and the date in the header, then the irradiation parameters for the examination and finally organ and tissue absorbed doses in mGy

Table 6. Organ and tissue absorbed dose output list of CALDose_X.

Institution: Local Hospital		
Patient: female, age: 55.6 years		
Name: Maria Silva		
Date: 26/6/2008		
Exposure conditions		
FAX06: Pelvis, anterior–posterior (AP)		
Image behind the body		
100 kVcp, 4.0 mm Al, 17 Deg Tungsten, IPEM/SR78		
Mean spectral energy: 51.4 keV, absorbed fraction: 0.57		
Source-to-detector (film): 106 cm		
Source-to-skin: 80 cm		
Field size in detector plane: 40 cm × 35 cm		
Field position: standard		
Charge: 24 mAs		
	Organ or tissue absorbed dose	
Organ/tissue	mGy	%
ESAK	3.85	1.32
Adrenals	0.07	7.64
Bladder wall	1.83	0.82
Colon wall	1.12	0.35
Breasts	0.00	4.69
Kidneys	0.26	0.87
Liver	0.04	0.95
Lungs	0.00	3.27
Ovaries	1.49	1.72
Pancreas	0.08	2.30
Small intestine wall	1.45	0.24
Skin entrance 7.2 cm × 7.2 cm	3.99	1.32
Spleen	0.07	2.42
Stomach wall	0.07	2.18
Uterus	1.28	0.71
Lymphatic nodes	1.44	0.34
BSC dose mainly in beam volume	3.30	0.19
RBM dose mainly in beam volume	1.19	0.24
Weighted female whole body dose	0.43	0.46
Risk of cancer incidence	3.93 cases	per 100000
Risk of cancer mortality	2.14 cases	per 100000

together with the statistical error of the Monte Carlo calculation. CALDose_X also provides the mean spectral energy and an 'absorbed fraction', which is the fraction of the emitted energy absorbed by the body. The last dose quantity shown in table 6 is the 'Weighted Female Whole Body Dose'. A similar quantity appears at the end of the corresponding list for the MAX06 phantom. According to ICRP103 (ICRP 2007), the arithmetic mean of these two sex-specific weighted absorbed doses is the effective dose. Finally, the last two entries show the patient's risk of cancer incidence and cancer mortality based on the risk coefficients given by the BEIR VII report (National Research Council 2005). The tables with the results can be printed and/or saved.

Options (b) and (d) are self-evident and are described in the user guide, which will be distributed with the CALDose_X software package.

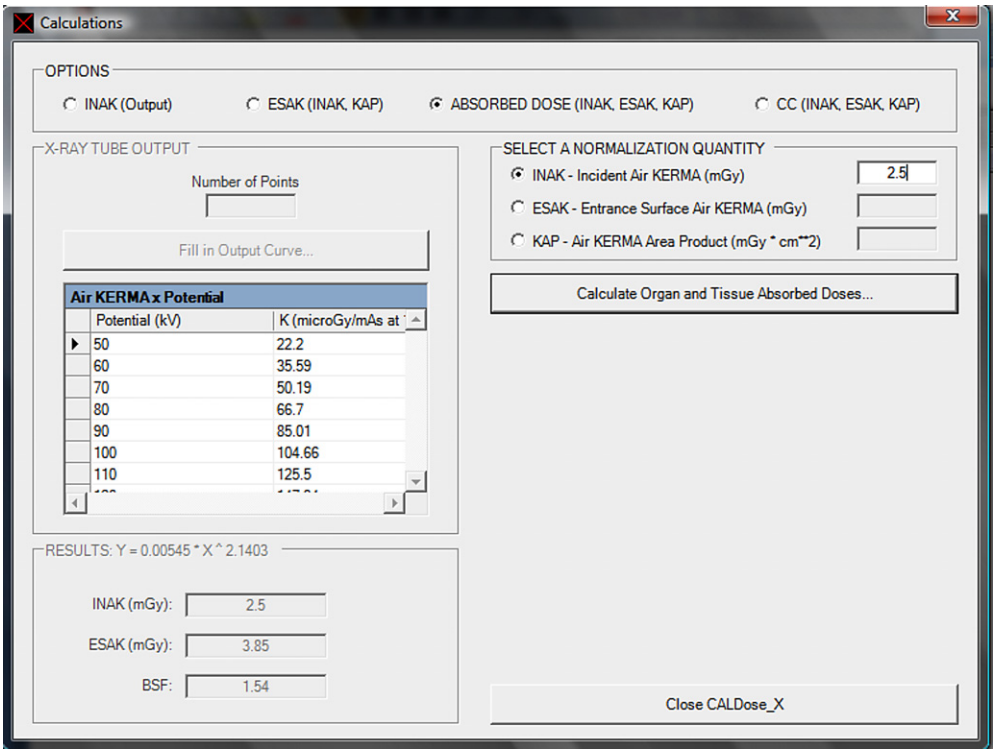

Figure 6. Third CALDose_X form: definition of the normalization quantity.

4. Conclusions

CCs between organ and tissue absorbed doses and the normalization quantities INAK, ESAK and KAP have been calculated with the MAX06 and the FAX06 phantoms for examinations frequently performed in x-ray diagnosis. Based on these CCs, the software tool CALDose_X has been developed, which can be used

- to calculate the INAK based on the output curve of the x-ray equipment;
- to assess the ESAK in order to control compliance with diagnostic reference levels;
- to calculate organ and tissue absorbed doses for patients with anatomies similar to the MAX06 and the FAX06 phantoms;
- to assess the effective dose based on ICRP103 and/or the patient's cancer risk based on the BEIR VII report;
- to demonstrate how organ and tissue absorbed doses, i.e. the radiation risk for the patient, depend on the proper selection of the exposure parameters. This information can be used in educational programs to train radiologists and technicians to understand how to perform x-ray examinations with the minimum exposure to the patient;
- to compare organ and tissue absorbed doses, effective doses or radiation risks from different radiological procedures, or from different x-ray units, or from different hospital, etc, to identify high- and low-risk examinations, or cases of good and bad practice; and
- to make risk assessments for surveys on radiological exposures, taking into account risk factors for the age and gender distribution of the patient population under consideration.

Uncertainties from the statistical error, the cross sections, the tissue compositions, the focus-to-skin distance and the measurement of the normalization quantities can easily sum up to about 65%. The field position can be very critical to organ and tissue absorbed doses and then there are also properties of the detector system, which can influence the organ and tissue absorbed doses, which have not been considered here. Therefore, an overall uncertainty of up to 100% is easily possible, without taking into account patient anatomies, which may deviate from the anatomies of the MAX06 and the FAX06 phantom. M Stabin has recently found similar estimates for internal dosimetry. He concluded that 'the combined uncertainties in any given radiopharmaceutical dose estimate are typically, at a minimum, a factor of 2 and may be considered greater, in general, because of normal human variability, and particularly in disease states' (Stabin 2008). According to Stabin, for therapeutic applications, this uncertainty can be reduced to 10–20%. Similar conditions exist for external medical exposures. In radiation therapy, where all exposure parameter are known and well under control, uncertainties can be made very small, while x-ray diagnosis unfortunately has to live with larger uncertainties. Still, reduction of uncertainties for CALDose_X is possible, especially by using adult phantoms with different fat distributions, which is already in preparation for the next update of the software.

Compared to MIRD5-based software tools for diagnostic radiology, CALDose_X presents two improvements: first, using two adult voxel phantoms allows for organ and tissue absorbed dose calculations based on a true to nature representation of the human anatomy as well as for the correct sex-specific calculation of the effective dose according to ICRP103 and, second, the cancer risk assessment offers an alternative to the effective dose, which cannot be used for an individual patient. The ICRP is currently preparing the publication of the adult reference computational phantoms. CALDose_X is a project that is open for the use of other adult and also pediatric phantoms in the future.

CALDose_X stands in the tradition of software tools developed earlier. It represents an improvement compared to them, but on the other hand it is only another milestone toward the aim of making such software tools for diagnostic radiology every time more patient specific.

Consequently, CALDose_X has to be understood as an open project, which will be updated from time to time with new features such as patient-specific fat distributions, age-related anatomical changes during adult life span, two updates, which would reduce some of the above-mentioned uncertainties, children phantoms, improved skeletal dosimetry, other types of examinations, etc.

CALDose_X and/or the phantoms FAX06 and MAX06 are available gratis from the following website of the Federal University of Pernambuco: http://www.grupodoin.com.

Acknowledgments

The authors would like to thank Dr John Kyriou for introducing the DoseCal software to our department and also for many interesting discussions on this subject. The authors would also like to thank the Conselho Nacional de Desenvolvimento Científico e Tecnológico—CNPq and the Fundação de Amparo à Ciência do Estado de Pernambuco—FACEPE for financial support.

References

Akahane K, Kai M, Kusama T and Saito K 2001 Dose estimation of patients from diagnostic x-ray based on CT-voxel phantom *Proc. 9th EGS4 Users' Meeting in Japan, KEK Proc. 2001-22* pp 87–91

Alderson S W, Lanzl L H, Rollins M and Spira J 1962 An instrumented phantom system for analog computation of treatment plans *Am. J. Roentgenol.* **87** 185

Birch R and Marshall M 1979 Computation of bremsstrahlung x-ray spectra and comparison with spectra measured with a Ge(Li) detector *Phys. Med. Biol.* **24** 505–17

Bozkurt A and Bor D 2007 Simultaneous determination of equivalent dose to organs and tissues of the patient and of the physician in interventional radiology using the Monte Carlo method *Phys. Med. Biol.* **52** 317–30

Brenner D and Huda W 2008 Effective dose: a useful concept in diagnostic radiology *Radiat. Prot. Dosim.* **128** 503–8

Cranley K, Gilmore B J, Fogarty G W A and Desponds L 1997 *Catalogue of Diagnostic X-ray Spectra and Other Data Report No. 78* (York: Institute of Physics and Engineering in Medicine)

Cristy M 1980 Mathematical phantoms representing children of various ages for use in estimates of internal dose *NUREG/CR-1159* (Tennessee: Oak Ridge National Laboratory)

Cristy M and Eckerman K F 1987 Dose–Response Functions for soft tissues of the skeleton *Specific Absorbed Fractions of Energy at Various Ages from Internal Photon Sources. I. Methods ORNL/TM-8381/V1* (Tennessee: Oak Ridge National Laboratory)

Drexler G, Panzer W, Widenmann L, Williams G and Zankl M 1990 The Calculation of Dose from External Photon Exposures Using Reference Human Phantoms and Monte Carlo Methods, Part III: Organ Doses in X-Ray Diagnosis (Institut für Strahlenschutz, GSF- Gesellschaft für Umwelt und Gesundheit, D-8042 Neuherberg, *GSF-Bericht S-11*, revised and amended version of S-1026, 1984)

Hart D, Jones D G and Wall B F 1994 Estimation of Effective Dose in Diagnostic Radiology from Entrance Surface Dose and Dose-Area Product Measurements (Chilton: National Radiological Protection Board)

Hubbell J H 1977 Photon mass attenuation and energy-absorption coefficients for H, C, N, O, Ar, and seven mixtures from 0.1 keV to 20 MeV *Radiat. Res.* **70** 58

ICRP 1991 1990 Recommendations of the international commission on radiological protection *ICRP Publication 60* (Oxford: Pergamon)

ICRP 1995 Basic anatomical and physiological data for use in radiological protection: the skeleton *ICRP Publication 70* (Oxford: Pergamon)

ICRP 1996 Conversion coefficients for use in radiological protection against external radiation *ICRP Publication 74* (Oxford: Pergamon) International Commission on Radiological Protection

ICRP 2003 Basic anatomical and physiological data for use in radiological protection: reference values *ICRP Publication 89* (Oxford: Elsevier) Ann. ICRP 32 (3–4)

ICRP 2007 Recommendations of the international commission on radiological protection *ICRP Publication 103* (Oxford: Elsevier) Ann. ICRP 37 (2–3)

ICRU 1989 Tissue substitutes in radiation dosimetry and measurement *ICRU Report No. 44* (Bethesda, MD: International Commission on Radiation Units and Measurements)

ICRU 2005 Patient dosimetry for X-rays used in medical imaging *ICRU Report No. 74* (Bethesda, MD: International Commission on Radiation Units and Measurements)

Jones D G and Wall B F 1985 Organ Doses from Medical X-ray Examinations Calculated Using Monte Carlo Techniques (Chilton: National Radiological Protection Board)

Jones D G 1995 Use of voxel phantoms in organ dose calculations *Proc. Int. Workshop on Voxel Phantom Development held at the National Radiological Protection Board (Chilton, UK, 6–7 July)*

Jones D G 1997 A realistic anthropomorphic phantom for calculating organ doses arising from external photon irradiation *Radiat. Prot. Dosim.* **72** 21–9

Kawrakow I 2000 Accurate condensed history Monte Carlo simulation of electron transport. I. EGSnrc, the new EGS4 version *Med. Phys.* **27** 485–98

Kawrakow I 2006 Version V4-r2–2-3 of the EGSnrc code system, http://www.irs.inms.nrc.ca/EGSnrc/EGSnrc.html

Ketel I J G, Volman M N M, Seidell J C, Stehouwer C D A, Twisk J W and Lambalk C B 2007 Superiority of skinfold measurements and waist over waist-to-hip ratio for determination of body fat distribution in a population-based cohort of Caucasian Dutch adults *Eur. J. Endocrinol.* **156** 655–61

Kramer R and Drexler G 1976 Zum Verhältnis von Oberflächen- und Körperdosis in der Röntgendiagnostik, 7. Wissenschaftliche Tagung der Deutschen Gesellschaft für Medizinische Physik e.V. Heidelberg, 5.-7.5.1976 *Medizinische Physik, Band* 2 Herausgegeben ed von W J Lorenz (Heidelberg: Hüthig Verlag) pp 683–95

Kramer R, Zankl M, Williams G and Drexler G 1982 The calculation of dose from external photon exposures using reference human phantoms and Monte Carlo methods. I: The male (ADAM) and female (EVA) adult mathematical phantoms *GSF-Report S-885* Institut für Strahlenschutz, GSF-Forschungszentrum für Umwelt und Gesundheit, Neuherberg-München

Kramer R, Vieira J W, Khoury H J, Lima F R A and Fuelle D 2003a All about MAX: a male adult voxel phantom for Monte Carlo calculations in radiation protection dosimetry *Phys. Med. Biol.* **48** 1239–62

Kramer R, Vieira J W, Lima F R A and Khoury J H 2003b Coeficientes de conversão para dose equivalente em órgãos e dose efetiva normalizadas pelo produto dose-área para radiografias do tórax usando o fantõma MAX *8th CONGRESSO BRASILEIRO DE FÍSICA MÉDICA Porto (Alegre/Brazil)*

Kramer R, Vieira J W, Khoury H J, Lima F R A, Loureiro E C M, Lima V J M and Hoff G 2004a All about FAX: a female adult voXel phantom for Monte Carlo calculation in radiation protection dosimetry *Phys. Med. Biol.* **49** 5203–16

Kramer R, Vieira J W, Khoury H J and Lima F R A 2004b MAX meets ADAM: a dosimetric comparison between a voxel-based and a mathematical model for external exposures to photons *Phys. Med. Biol.* **49** 887–910

Kramer R, Khoury H J and Vieira J W 2005a Comparison between effective doses for voxel-based and stylized exposure models from photon and electron irradiation *Phys. Med. Biol.* **50** 5105–26

Kramer R, Santos A M, Brayner C A O, Khoury H J, Vieira J W and Lima F R A 2005b Application of the MAX/EGS4 exposure model to the dosimetry of the Yanango radiation accident *Phys. Med. Biol.* **50** 3681–95

Kramer R, Khoury H J, Vieira J W and Lima V J M 2006a MAX06 and FAX06: Udate of two adult human phantoms for radiation protection dosimetry *Phys. Med. Biol.* **51** 3331–46

Kramer R, Khoury H J, Lopes C and Vieira J W 2006b Equivalent dose to organs and tissues in hysterosalpingography calculated with the FAX (Arch. Histol. Cytol.emale Adult voXel) phantom *Br. J. Radiol.* **79** 893–8

Kramer R, Khoury H J, Vieira J W and Kawrakow I 2006c Skeletal dosimetry in the MAX06 and the FAX06 phantoms for external exposure to photons based on vertebral 3D-microCT images *Phys. Med. Biol.* **51** 6265–89

Kramer R, Khoury H J, Vieira J W and Kawrakow I 2007 Skeletal dosimetry for external exposure to photons based on μCT images of spongiosa from different bone sites *Phys. Med. Biol.* **52** 6697–716

Kyriou J C, Newey V and Fitzgerald M C 2000 *Patient Doses in Diagnostic Radiology at the Touch of a Button* (London: The Radiological Protection Center, St. George's Hospital)

Kyriou J C 2008 Private communication

Le Heron J C 1992 Estimation of effective dose to the patient during medical x-ray examinations from measurements of the dose-area product *Phys. Med. Biol.* **37** 2117–26

Lima F R A, Kramer R, Vieira J W and Khoury J H 2003 Organ dose conversion coefficients for lumbar spine examinations calculated for the MAX phantom *Radiation Protection Symposium of the North West European Rp Societies 2003, Utrecht. Extended Abstracts of the Radiation Protection Symposium of the North West European RP Societies (Utrecht, The Netherlands)*

Lima F R A, Kramer R, Vieira J W, Khoury H J, Loureiro E C M and Hoff G 2004 Effective dose conversion coefficients with gender-specific, adult voxel phantoms for radiographic examinations common in diagnostic radiology *11th Int. Congress of the International Radiation Protection Association (Madrid, Spain, 23–28 May 2004)*

National Research Council 2005 *Health Risks from Exposure to Low Levels of Ionizing Radiation – BEIR VII.* (Washington, DC: The National Academies Press)

Nelson W R, Hirayama H and Rogers D W O 1985 The EGS4 Code System SLAC-265, Stanford Linear Accelerator Center, Stanford University, Stanford, CA, USA

PCXMC 2008 http://www.stuk.fi/sateilyn_kayttajille/ohjelmat/PCXMC/en_GB/pcxmc/,Accessed 28 April 2008

Petoussi-Henss N, Panzer W, Zankl M and Drexler G 1995 Dose-area product and body doses *Radiat. Prot. Dosim.* **57** 363–6

Petoussi-Henss N, Zankl M and Panzer W 2005 Estimation of organ doses in radiology using voxel models describing different patients *Biomed. Tech.* **50** 664–5 Suppl. 1

Rannikko S, Ermakov I, Lampinen J S, Toivonen M, Karila K T K and Chervjakov A 1997 Computing patient doses of X-ray examinations using a patient size- and sex- adjustable phantom *Br. J. Radiol.* **70** 708–18

Rosenstein M 1976 *Organ Doses in Diagnostic Radiology* (US Department of Health, Education and Welfare, Bureau of Radiological Health, BRH Tech Publ DA 76-8030) (Rockville, MD: Bureau of Radiological Health)

Rosenstein M 1988 *Handbook of Selected Tissue Doses for Projections Common in Diagnostic Radiology* (US Department of Health, Education and Welfare, Bureau of Radiological Health, BRH Tech Publ DA 89-8031)

Schultz F W, Geleijns J and Zoetelief J 1994 Calculation of dose conversion factors for posterior–anterior chest radiography of adults with a relatively high-energy X-ray spectrum *Br. J. Radiol.* **67** 775–85

Schultz F W, Geleijns J and Zoetelief J 1995 Effective doses for different techniques used for PA chest radiography *Radiat. Prot. Dosim.* **57** 371–6

Servomaa A and Tapiovaara M 1998 Organ dose calculation in medical X-ray examinations by the program PCXMC *Radiat. Prot. Dosim.* **80** 213–9

Snyder W S, Ford M R, Warner G G and Watson G G 1974 Revision of MIRD Pamphlet No 5 Entitled 'Estimates of absorbed fractions for monoenergetic photon sources uniformly distributed in various organs of a heterogeneous phantom *ORNL-4979* (Tennessee: Oak Ridge National Laboratory)

Stabin M 2008 Uncertainties in internal dose calculations for radiopharmaceuticals *J. Nucl. Med.* **49** 853–60

Tapiovaara M 2008 Private communication
Vieira J W, Lima F R A, Kramer R and Khoury J H 2003 Organ and tissue equivalent doses from abdominal X-ray examinations calculated with the MAX/EGS4 exposure model IRPA VI Latin American Regional Congress 2003 (Lima /Peru) Anais do VI Congresso sobre Seguridad Radiologica y Nuclear
Wendin L 2008 Private communication
Williams G, Zankl M, Abmayr W, Veit R and Drexler G 1986 The calculation of dose from external photon exposures using reference and realistic human phantoms and Monte Carlo methods *Phys. Med. Biol.* **31** 347–54
WinODS 2008 http://www.rti.se/download_software/index.html Accessed 28 April 2008
Winslow M, Huda W, Xu X G, Chao T C, Shi C Y, Ogden K M and Scalzetti M 2004 Use of the VIP-man model to calculate energy imparted and effective dose for X-ray examinations *Health Phys.* **86** 174–82
Zankl M, Panzer W and Herrmann C 2000 Calculation of patient doses using a human voxel phantom of variable diameter *Radiat. Prot. Dosim.* **90** 155–8
Zankl M and Wittmann A 2001 The adult male voxel model GOLEM segmented from whole-body CT patient data *Radiat. Environ. Biophys.* **40** 153–62